

STRUCTURE AND ADHESIVE PROPERTIES OF NANOCOMPOSITES BASED ON FUNCTIONALIZED NANOFILLERS

Anatoly SVIRIDENOK*, Aliaksei KRAUTSEVICH*, Olga MAKARENKO**, Vladimir VOINA***

*Research Center of Resource Saving Problems of National Academy of Sciences of Belarus,
Tizenhauza sq., 7, 230023 Grodno, Belarus,

**V.A. Belyi Metal-Polymer Research Institute of National Academy of Sciences of Belarus,
32a Kirov Str., 246050 Gomel, Belarus

***Yanka Kupala State University of Grodno, Ozhetsko Str., 22, Grodno, Belarus

resource@mail.grodno.by, krautsevich_a@tut.by, olga-mpri@mail.ru, kaf_physics@grsu.by

Abstract: Nanocomposite samples of the copolymer of ethylene and vinyl acetate containing carbon nanofibers and nanotubes have been prepared by mixing in solution. In order to improve interfacial interactions in the polymer-nanofiller system they were subjected to a preliminary chemical functionalization. The efficiency of functionalization was estimated by the IR spectroscopy. The X-ray diffraction and strength characteristics of the obtained nanocomposites filled by the untreated and functionalized carbon nanofibers and nanotubes with different filling degree were compared.

1. INTRODUCTION

Carbon nanomaterials (CNM) are considered to be promising fillers for nanocomposites thanks to their high mechanical, adhesive and other properties. These properties may improve essentially technical characteristics of nanocomposites (Cipiriano, 2007; Yang, 2004). It is, nevertheless a difficult task to create such a nanocomposite. The difficulties in application of nanostructured nanofillers consist in attaining their optimal dispersion in the matrix polymer, and the efficient bonding with the polymer macromolecules. The most applicable method of reaching the optimal dispersion of nanofillers is the exposure to the ultrasonic field (Kodgire, 2006; Lin, 2005). The method of efficient fixing of the single-wall (Bahr, 2002; Dyke, 2004; Haggemueller et al, 2006) and multiwalled (Mago et al, 2008; Lin, 2002; Grimes, 2001) nanotubes in the polymer matrix consists in their preliminary covalent functionalization by the polar groups. There is, however lack of information on the expediency and possibility of functionalizing carbon nanomaterials in the form of a mixture of nanofibers and nanotubes.

In the present work the nanofiller was introduced into the polymer matrix by the method of mixing in solution. This method is considered in literature as a most efficient one for obtaining CNM-filled nanocomposites. And as reported in some scientific papers (Mark, 2005) this method most enables to solve the problem of nanoparticles agglomeration at introduction into the polymer matrix and to ensure a better interfacial interaction between the polymer matrix and nanofiller particles.

2. EXPERIMENTAL DETAILS

2.1. CNM and its functionalization

The CNM used in the present investigations was derived by methane decomposition under a high-voltage discharge

plasma in the Institute of Heat and Mass Transfer of NASB. It is a soot-like matter consisting of carbon nanofibers, nanotubes as well as the particles of amorphous and graphitized carbon. The dimensions of CNM nano-structures were determined from the SEM micrographs.

The functionalized CNM (f-CNM) was obtained by treating with a mixture of concentrated mineral acids. The CNM were treated with the acids during 3-4 hours under 80 ± 5 °C with constant agitation, followed by cooling and settling of the mixture. Thus produced precipitant was washed repeatedly by distilled water and dried till the full removal of the water.

2.2. Preparation of the nanocomposites

The polymer matrix under study was the copolymer of ethylene and vinyl acetate (EVA) produced by OAO SEVILEN (Kazan, Russia), grade 11808-340 with vinyl acetate content 26-30 wt%. The nanocomposite was prepared by mixing CNM in the EVA solution in oxygen AT exposure to the ultrasonic field. With this aim, the EVA granulate was placed into a flask with a slice, and a necessary amount of CNM ($0 \div 0,5$ wt%) with a solvent. The flask was placed into an ultrasonic bath Bandelin Sonorex Super (of 80 Wt power and 35 kHz frequency) fit with a heater. The polymer was dissolved under $50 \div 55$ °C within 1 h. To avoid gaseous losses of the solvent a backflow condenser was installed in the slice inside the flask. The CNM nanofiller was subjected to the ultrasonic dispersion for 30 min after complete dissolving of the polymer. The prepared solutions of EVA with suspended in them CNM were poured into the Petri dishes and placed into an exhaust hood for 12 hours. Then, the dishes were placed into a thermostat under 60 °C temperature for a day. The resultant dry precipitant was milled. Seven samples of nanomodified EVA with CNM and f-CNM content $0 \div 0,5$ wt% were prepared following above procedure. To produce experimental samples of glued EVA splices

and to continue the investigations, thus obtained nanocomposites were ground into a powder using a cryogenic mill "Pulverisette-14" and a vibration feeder "Laborette-24" for continuous feeding of the ground material. Liquid nitrogen was used as a cooling agent. The composite material ground into the powder was then dried at 10 °C temperature during 8 hours to remove condensation water.

To study the effect of CNM nanofiller on structural parameters of the EVA matrix, the prepared powder nanocomposites underwent hot pressing to obtain 200-250 μm thick films.

To define variations in adhesive properties of EVA towards metal surfaces induced by introduction of CNM, we have prepared model samples of glued joints from the powder nanocomposites. The metal surfaces for gluing were strips of aluminum sheets having width $b = 200$ mm, and thickness $h \approx 0,2$ mm. The strips were glued with overlap to the EVA nanocomposite by hot pressing under above 130 °C. The overlapping length was $a = 150$ mm, thickness of the glue joint $t \approx 200$ μm (Fig. 1). The samples were prepared and the adhesive bond was tested for the ultimate strength at shear following the State Standard GOST 14759-69 "Glue joints of metals. A method for determining shear strength". (Airapetyan, 1980). The maximal load on the adhesive bond till failure by shear was estimated on a testing machine Instron 5567 at velocity of the grips 10 mm/min.

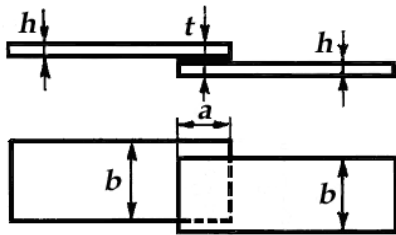


Fig. 1. Scheme of a sample from aluminum sheets with a glue joint on EVA nanocomposite

2.3. Investigation methods

The efficiency of CNM functionalization was estimated by the IR spectra recorded by a spectrophotometer Nicolet 5700 FTIR. The spectra were recorded on a NaCl glass.

The radiograms of the composite films were recorded using diffractometer Dron-2,0 with radiation of $\text{CuK}\alpha$, filtered $\lambda = 0,1542$ nm. The X-ray diffraction parameters were obtained by processing the radiograms keeping to the traditional procedures.

It is common knowledge (Jale, 1968; Martynov, 1972) that the presence of a clearly isolated diffusion halo and narrow reflexes on the radiogram assists in defining radiologic crystallinity degree ω_c by the relation:

$$\omega_c = \frac{\int_{\Theta_1}^{\Theta_2} S^2 J_c(S) dS}{\int_{\Theta_1}^{\Theta_2} S^2 J(S) dS}, \quad (1)$$

where $S = 2\sin\Theta/\lambda$ – vector of reciprocal space; J – total scattering intensity of X-ray beams in the interval of angles Θ_1 and Θ_2 ; J_c – total scattering intensity in the region of narrow reflexes.

The interplanar distances corresponding to the reflexes were determined by Bregg-Wolf's formula (Wanderlich, 1976):

$$\frac{d}{n} = \frac{\lambda}{2 \sin \Theta_b}, \quad (2)$$

where d – distance between planes of reflection; n – whole number; Θ_b – the angle formed by the incident beam and the plane; in our case $n = 1$; $\lambda = 1,514$ Å.

The dimensions of crystallites were calculated by Sherrer's formula (Martynov M.A., 1972):

$$L = \frac{0,9\lambda}{\beta \cdot \cos \Theta_b}, \quad (3)$$

where L – crystallite size, Å; β – line width, radian; λ – wavelength, Å.

The radiograms were recorded on a chart strip with recalculation so as to consider the scale. In our case, one angular degree corresponded on the strip to a 6 mm distance, one radian corresponded to the angle 57,3°. So, Eq. (3) for value L expressed in Å, will take the form:

$$L = \frac{0,9 \cdot 1,542 \text{ Å} \cdot 6 \text{ mm} \cdot 57,3^\circ}{\beta_{\text{mm}} \cdot \cos \Theta_b}. \quad (4)$$

To describe the changes in the supermolecular structure of the matrix in response to nanofiller effects, one should study the following parameters: relative share of the coarse crystals in the crystalline region δ_b :

$$\delta_b = \frac{S_3}{S_2 + S_3} \quad (5)$$

where S_2 ; S_3 are the integral intensities of reflexes 2 and 3, respectively; the relative share of the fine crystals δ_s in the amorphous region determined by:

$$\delta_s = \frac{S_2}{S_2 + S_{am}} \quad (6)$$

where S_2 , S_{am} are the integral intensities of reflex 2 and the amorphous region, correspondingly.

3. RESULTS AND DISCUSSION

3.1. CNM and results of its functionalization

SEM investigations (Fig. 2) have shown that the CNM consists of 100÷200 nm in diameter and 1÷1.5 μm long carbon nanofibers; multiwall carbon nanotubes 20÷40 nm in diameter and 1÷10 μm long in the form of a branched interweaving. Notice that the particles of the amorphous and nanotube carbon are seen on all SEM microphotographs. Proceeding from the above, we can say that CNM

is a polydispersed product containing different in shape and size nanoparticles with the admixture of microparticles and amorphous carbon nanoparticles.

The CNM and f-CNM were characterized using the method of IR spectroscopy. There were no any essential differences after CNM treating with a mixture of mineral acids (Fig. 3). Both curves display the bands in the region 1725 cm^{-1} that correspond to oscillations of the C=O link in carboxyl and a wide peak between 3000 and 3600 cm^{-1} correlated with hydroxide (-OH) oscillations in carboxyl. The appearance or intensification of named bands in the same regions was also observed in the works (Hung, 2009 and Anoshkin, 2008) after the acid treatment of nanotubes and nanofibers. Proceeding from these results, we may assume that there is insignificant content of polar groups on the surface of nanostructures of the initial CNM, while the acids treatment augments their amount.

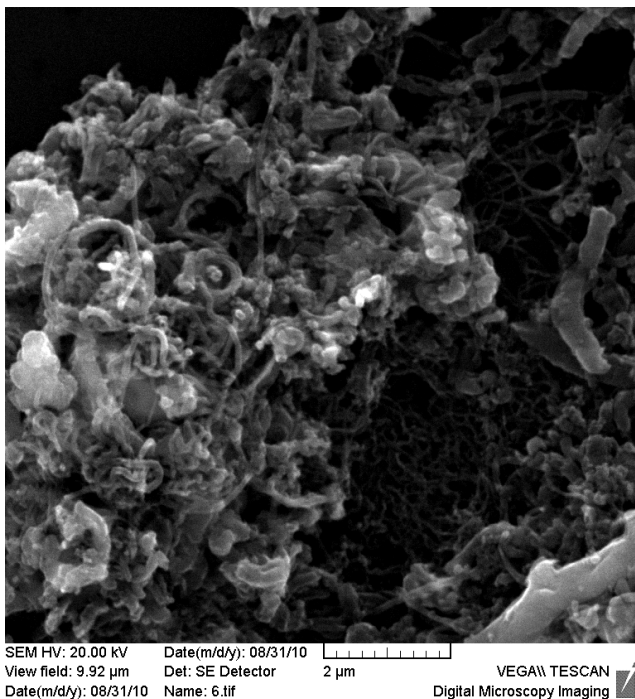


Fig. 2. SEM image of CNM

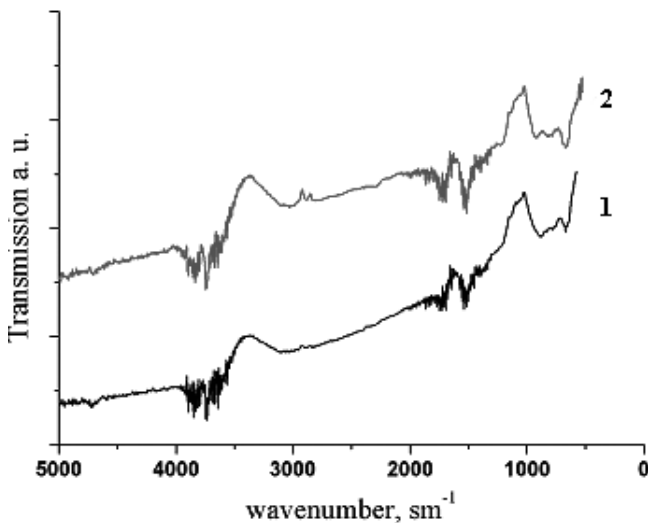


Fig. 3. IR spectra of CNM (1) and f-CNM (2)

3.2. X-ray diffraction parameters of the nanocomposite

Fig. 4 presents most typical radiograms of the non-filled EVA film, nanocomposite EVA + CNM films and those of EVA + f-CNM. The radiogram of the EVA film displays a single clear-cut reflex 2 and a considerable area of a symmetric amorphous halo. In the case with the nanocomposite films, their radiograms show reflexes 1, 3, 4 and reduced a little area of the amorphous halo, which is a proof to variations in the supermolecular structure of the nanocomposite. The essential differences in radiograms of the films EVA and f-CNM consist in the absolute and relative intensities of some reflexes, as well as the shape and size of the amorphous halo. It should be noted that the number of reflexes and their angular position on the radiograms is similar for all samples under study (within the limits of test sensitivity and measurement errors).

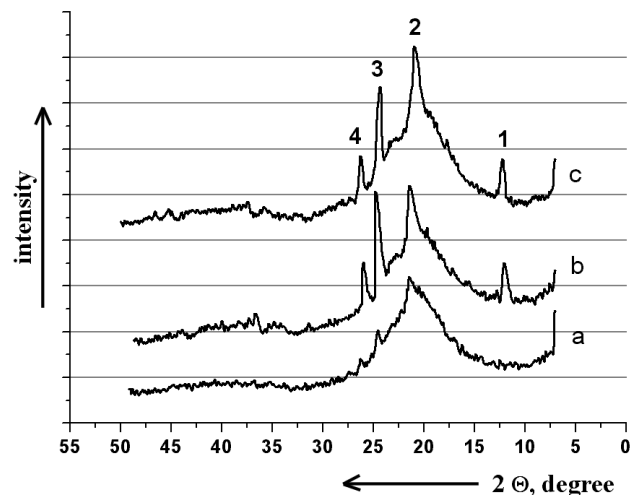


Fig. 4. Characteristic radiograms of the films: a –EVA, b – EVA + CNM); c – EVA +f-CNM

Tab. 1. X-ray diffraction parameters of films EVA

Samples	Struct. parameter	Reflex No.				α_c
		1	2	3	4	
EVA (granulate)	2θ	weak	$21^\circ33'$	$24^\circ66'$	weak	0,11
	$d, \text{Å}$	-	2,12	1,85	-	
	$L, \text{Å}$	-	47	210	-	
EVA (from solution)	2θ	weak	$21^\circ33'$	$24^\circ66'$	weak	0,11
	$d, \text{Å}$	-	2,12	1,85	-	
	$L, \text{Å}$	-	73	276	-	
EVA + CNM 0,1 wt%	2θ	$12^\circ20'$	$21^\circ20'$	$24^\circ66'$	$26^\circ50'$	0,16
	$d, \text{Å}$	3,65	2,13	1,85	1,73	
	$L, \text{Å}$	163	73	210	247	
EVA+ f-CNM 0,1 wt%	2θ	$12^\circ20'$	$21^\circ20'$	$24^\circ66'$	$26^\circ50'$	0,22
	$d, \text{Å}$	3,65	2,13	1,85	1,73	
	$L, \text{Å}$	122	63	210	267	

The calculated X-ray structural parameters of the samples are shown in Tab. 1.

The calculations using formula (4) have shown that the crystalline phase in the studied samples consists of rather

fine crystals $47 \div 73 \text{ \AA}$ (reflex 2), average ones $122 \div 163 \text{ \AA}$ (reflex 1) and coarse crystals $210 \div 276 \text{ \AA}$ (reflexes 3 and 4). A negligible effect is imposed on the crystal size by preliminary dissolving of the polymer matrix in the organic solvent. The crystals are a little larger in these films. Introduction of CNM into the EVA matrix forces the coarse crystals to return from 276 down to 210 \AA size, i.e. to the size similar to the initial EVA not subjected to preliminary dissolving.

The calculation of crystallinity degree (α_c) using formula (1) has shown that the non-filled EVA films have $\alpha_c = 0,11$. Introduction of CNM into the EVA matrix increases the degree of crystallinity, while the maximal value of $\alpha_c = 0,24$ was reached in the EVA samples with 0,5 wt% concentration of f-CNM.

Depending on the content (wt%) and the type of CNM in these films EVA differently changes the ratio of large and small crystals. Figure 5 presents the dependence of the fraction of small crystals in the amorphous region.

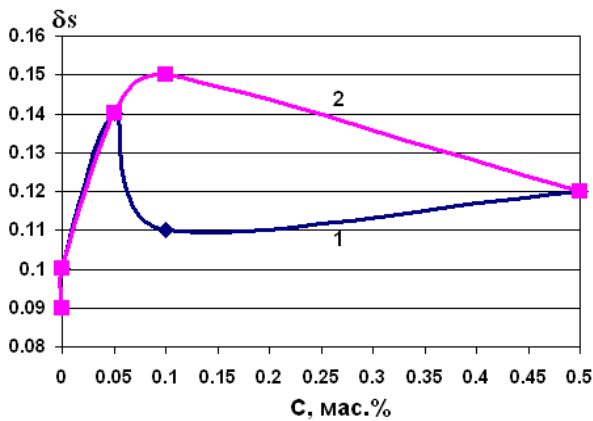


Fig. 5. Variations in relative share of fine crystals in the amorphous phase depending on the wt% content of nanofiller in EVA + CNM (1) and EVA + f- CNM films (2)

The introduction of all types of CNM leads to an increase in the relative share of small crystals in the amorphous region. The maximum value of the relative share of small crystals is achieved for films of EVA f-CNM at a concentration of 0,1 wt.%. Similar variations in the polymer crystal dimensions upon introduction of functionalized carbon nanoparticles were observed by other researchers on the example of polybutylene terephthalate (Mago et al., 2008). The relative share of the coarse crystals in the nanocomposite EVA films increased too, and there were not any noticeable differences between the films EVA + CNM or EVA and f-CNM in what concerns this parameter.

Based on the results obtained, we have made the following conclusions. The major effect induced by the CNM introduction is the formation of a fine-crystalline phase. It is to be noted that the layer-to-layer distance in the fine crystals (reflex 2, $d = 2,12 \text{ \AA}$) coincides with the mean interlayer distance in the amorphous phase. Such a situation may occur if the crystalline region created by the unrolled molecular balls, in which the straightened macromolecular chains are forming the crystals (Wanderlich, 1976). Named structures are characterized by the presence of a large num-

ber of transit chains, which improves in a number of cases physico-mechanical characteristics. The nanostructures f-CNM assist most efficiently the formation of crystals from the straightened macromolecular chains when their concentration is 0,1 wt%.

3.3. Adhesive properties of the nanocomposite

The results of testing mechanical properties of the glue joints in which EVA was used for lap splicing of aluminum sheets are shown in Table 2.

The data proves that introduction of CNM into the EVA matrix enhances strength of the glue joint. Most strong glue joints with EVA are obtained when the f-CNM is used as a filler, which is evidently related to optimization of the interfacial interactions in the nanofiller-matrix contact.

Tab. 2. Mechanical test results of glue joints with EVA at shear

Glue joint composition	Ultimate load to failure	Ultimate strength, MPa	Strength variation related to check sample, %
EVA (check)	42.5	14.2	–
EVA + CNM 0,05 wt%	52.4	17.5	23.2
EVA + CNM 0,1 wt%	51.4	17.1	20.9
EVA + f-CNM 0,05 wt%	55.1	18.4	29.7
EVA + f-CNM 0,1 wt%	57.3	19.1	34.9

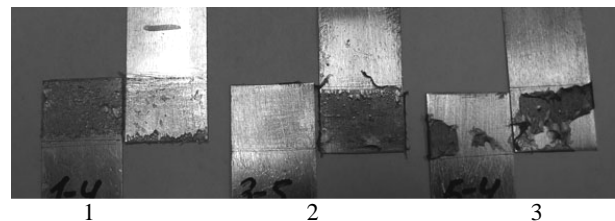


Fig. 6. Failure mode of glue joints: 1 – CNM; 2 – EVA + CNM; 3 – EVA + f-CNM

It should be noted that the majority of the test samples has shown the adhesive failure mode in the glue joints. As for the samples containing EVA and f-CNM, they show simultaneously the signs of adhesive and cohesive failure in the splice (Fig. 6). This fact speaks in favor of the increasing adhesive strength.

4. CONCLUSIONS

The test results have proved that the acid treatment augments the content of polar groups in the CNM on the surface of nanostructures. All nanomodified samples display the enhanced crystallinity degree, its maximum being observed in the case of using the f-CNM. The crystal-

linity degree growth takes place mainly due to the increasing amount of fine crystals in the amorphous region. The maximal strength increase by $\approx 35\%$ in the glue joint with the EVA nanocomposite was recorded when f-CNM was introduced.

REFERENCES

1. **Airapetyan L. H.** (1980), *Ref. book on glues*, Leningrad, Khimiya.
2. **Anoshkin I. V.** (2008), *Chemical modification and fractioning of thin multilayered carbon nanotubes*, Dissertation, Rus. Chem.-Technol. Univ. named after D.I. Mendeleev.
3. **Bahr J. L.** (2002), Covalent chemistry of single-wall carbon nanotubes, *J. Mater. Chem.*, Vol. 1952–1958.
4. **Cipiriano B. H.** (2007), Effects of aspect ratio of MWNT on the flammability properties of polymer nanocomposites, *Polymer*, Vol. 48, 6086–6096.
5. **Hung N.Ch.** (2009), Modification of carbon nanotubes and nanofibers for obtaining ceramic nanocomposites. Dissertation, Rus. Chem.-Technol. Univ. named after D.I. Mendeleev.
6. **Jale F.H.** (1968), *Polymer monocrystals*, Moscow, Khimiya.
7. **Dyke C. A.** (2004), Covalent functionalization of single-wall carbon nanotubes for materials applications, *J. Phys. Chem. A.*, Vol. 108, 11151–11159.
8. **Grimes C. A.** (2001), Effect of purification of the electrical conductivity and complex permittivity of multiwall carbon nanotubes, *J. of Applied physics*, Vol. 90, No 8, 4134–4137.
9. **Haggenmueller R.** (2006), Interfacial in situ polymerization of single wall carbon nanotube/nylon 6,6 nanocomposites, *Polymer*, Vol. 47, 2381–2388.
10. **Kodgire P. V.** (2006), Control of multiwall carbon nanotubes dispersion in polyamide6 matrix: An assessment through electrical conductivity, *Chemical Physics Letters*, Vol. 432, 480–485.
11. **Lin T. S.** (2005), Percolated network of entangled multi-walled carbon nanotubes dispersed in polystyrene thin films through surface grafting polymerization, *Materials Chemistry and Physics*, Vol. 94, Is. 2-3, 438–443.
12. **Lin Y.**, (2002), Functionalizing Multiple-Walled Carbon Nanotubes with Aminopolymers, *Journal of Physical Chemistry B*, Vol. 106, No. 6, 1294–1298.
13. **Mago G.** (2008), Effect of Functionalization on the Crystallization Behavior of MWNT-PBT Nanocomposites, *Mater. Res. Soc. Symp. Proc.*, Vol. 1056, 1–6.
14. **Mark K.** (2005), Shear modification of HDPE-clay nanocomposites, *United States Patent*, No 6,884,834.
15. **Martynov M. A.** (1972), *Radiography of polymers*, Moscow, Khimiya.
16. **Wanderlich B.** (1976), *The physics of macromolecules*, Moscow, Mir.
17. **Yang J.** (2004), Fabrication and Characterization of Soluble Multi-Walled Carbon Nanotubes Reinforced P(MMA-co-EMA) Composites, *Macromol. Mater. Eng.*, Vol. 289, 828–832.